ACS APPLIED MATERIALS & INTERFACES

Research Article

www.acsami.org

Ultrafine Pd Nanoparticles Encapsulated in Microporous Co_3O_4 Hollow Nanospheres for In Situ Molecular Detection of Living Cells

Jiangbo Xi,[†,§] Yan Zhang,[†,§] Ning Wang,[‡] Lin Wang,[‡] Zheye Zhang,[†] Fei Xiao,*[,†] and Shuai Wang*[,†]

[†]School of Chemistry and Chemical Engineering, Huazhong University of Science and Technology, Wuhan, 430074, P. R. China

[‡]Center for Tissue Engineering and Regenerative Medicine, Union Hospital, Tongji Medical College, Huazhong University of Science and Technology, Wuhan, 430022, P. R. China

Supporting Information

ABSTRACT: Recent progress in the in situ molecular detection of living cells has attracted tremendous research interests due to its great significance in biochemical, physiological, and pathological investigation. Especially for the electrochemical detection of hydrogen peroxide (H_2O_2) released by living cells, the highly efficient and cost-effective electrocatalysts are highly desirable. In this work, we develop a novel type of microporous Co_3O_4 hollow nanospheres containing encapsulated Pd nanoparticles (Pd@Co_3O_4). Owing to the synergy effect between the permeable microporous Co_3O_4 shell and the ultrafine Pd nanoparticles that encapsulated in it, the resultant Pd@Co_3O_4 based electrode exhibits excellent electrochemical sensor performance toward H_2O_2, even when the content of Pd in Pd@Co_3O_4 hollow nanospheres is as low as 1.14 wt %, which enable it be used for real-time tracking of the secretion of H_2O_2 in different types of living human cells.

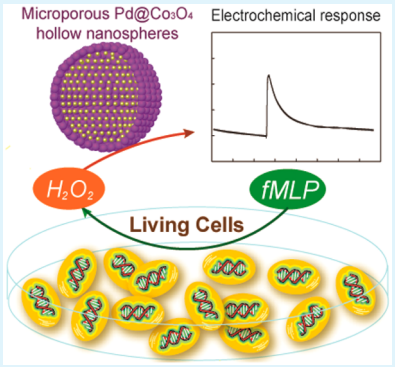

KEYWORDS: *microporous hollow nanospheres, ultrafine Pd nanoparticles, electrochemistry, biosensors, living cell tracking*

1. INTRODUCTION

Reactive oxygen species (ROS), including superoxide anion ($O_2^{\bullet-}$), hydrogen peroxide (H_2O_2), hydroxyl radical ($OH^{\bullet}$), and peroxynitrite ($ONOO^-$), have attracted great attention due to their important roles in the metabolism process.[1,2] H_2O_2 is one of the most stable ROS and the product of $O_2^{\bullet-}$ dismutation from superoxide dismutase. The physiological levels of H_2O_2 are closely associated with the degradation and formation of reactive free radicals, such as $O_2^{\bullet-}$ and $^{\bullet}OH$. Excessive H_2O_2 is implicated in arteriosclerosis, cancer, stroke, diabetes, and a host of other serious diseases.[3] Therefore, it is of great importance to monitor the H_2O_2 level in a biological environment, especially in a cellular environment. Nowadays, several analytical techniques have been developed for the determination of H_2O_2, such as fluorometry,[4,5] spectrophotometry,[6] chromatography,[7] and electrochemistry.[8] Among these techniques, electrochemical methods are more suitable for in situ and real-time analysis of H_2O_2 due to their fast response, high sensitivity, good selectivity, facile operation, and excellent reproducibility.[8] Electrochemical methods are usually based on the catalytic reduction of H_2O_2 by the natural enzyme, for example, horseradish peroxidase, which shows high catalytic efficiency and selectivity toward H_2O_2;[9−11] however, the immobilization and stabilization protocol of the enzyme on the electrode is very complicated. Moreover, the activity of the enzyme electrode is easy to reduce or even deactivate.[12] In this case, noble metals (Pt, Pd, Ag, and Au) and their alloys have been explored as the substitute of enzyme for H_2O_2 detection due to their high catalytic activity toward the direct electrochemical oxidation/reduction of H_2O_2.[13] Especially, tremendous efforts have been stimulated to the design and synthesis of Pd nanoparticles (NPs) owing to their size- and shape-dependent electrocatalytic performance,[14−16] which gives rise to a significant improvement for nonenzymatic electrochemical sensing of H_2O_2.[17] Nevertheless, in the design and application of these metal NP catalysts, the technologically crucial issue is the undesirable coalescence, sintering, aggregation, or corrosion/dissolution of NPs, which causes a rapid decay in catalytic abilities.[18−20] On the other hand, for electrocatalytic applications, it is necessary to load noble metal NPs on an electrode with high density in order to achieve large active surface areas and high catalytical activity, which would inevitably increase the cost of the metal catalyst. Therefore, it is still a challenge to develop low-load noble metal NPs without sacrificing the high catalytical activity, in view of improving the efficiency and cost-effectiveness of a catalytic process.

To overcome these challenges, in this work, we develop a novel type of Pd-based nanocatalyst, i.e, microporous Co_3O_4 hollow nanospheres containing encapsulated Pd NPs (Pd@Co_3O_4), and explored its practical application as the electrode material in an electrochemical sensor for the nonenzymatic detection of H_2O_2 released by living cells. Previous works have also demonstrated that loading Pd nanoparticles on a large-surface-area and porous substrate is an effective way to enhance

Received: January 20, 2015
Accepted: February 23, 2015
Published: February 23, 2015

DOI: 10.1021/acsami.5b00600
ACS Appl. Mater. Interfaces 2015, 7, 5583−5590

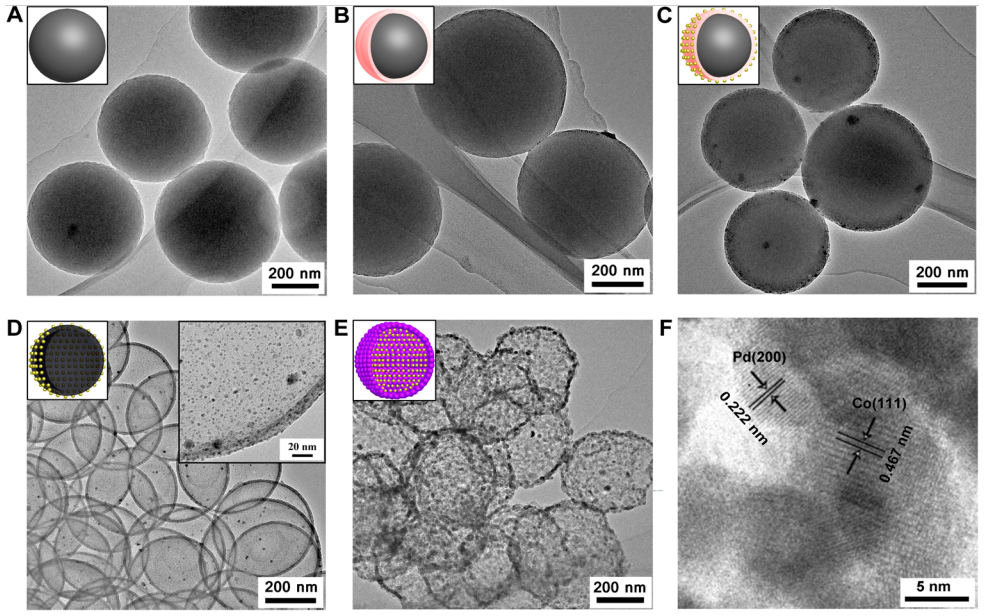

Figure 1. TEM images of (A) SiO_2 spheres, (B) SiO_2@PDA spheres, (C) SiO_2@PDA@Pd spheres, (D) C@Pd hollow spheres, and (E) Pd@Co_3O_4 hollow spheres and (F) HRTEM image of Pd@Co_3O_4 hollow spheres.

the electrocatalytic activity and improve the nonenzymatic sensing performance toward the H_2O_2.[21] Recently, significant efforts have been devoted to fabricating hollow spheres with hierarchical core−shell structure owing to their multifunctional use in a myriad of fields, including surface enhanced Raman scattering (SERS), photocatalysis, drug delivery, Li-ion battery, and nanoreactor.[22−33] For electrocatalytic application, the core−shell structured materials can effectively prevent the encapsulated catalytic active species from aggregation or leaching by the shell protection.[34] Meanwhile, the hollow nanospheres with microporous shells provide a large surface area for catalytic reaction as well as promote diffusion and mass transfer of reactants, which allow better reaction kinetics at the electrocatalyst surface. Owing to the synergy effect between the permeable microporous Co_3O_4 shell and the active Pd NPs encapsulated in it, the resultant Pd@Co_3O_4 based electrochemical sensor shows significantly improved electrocatalytic activity toward H_2O_2 as well as high sensitivity, even when the content of Pd in Pd@Co_3O_4 hollow nanospheres is as low as 1.14 wt %. These outstanding features, combined with its excellent stability and reproducibility, enable it to be used for real-time tracking of the secretion of H_2O_2 in living cells, i.e., human cervical carcinoma Hela cell, RSC96 Schwann cells, and human umbilical vein endothelial cells (HUVEC). These allow the Pd@Co_3O_4 based biosensor to contribute to the full realization of a high-performance biosensor for physiological and pathological monitoring of H_2O_2.

2. EXPERIMENTAL SECTION

2.1. Materials. All solutions were prepared using deionized water (resistivity >18 Ω·cm^{-1}). *N*-Formyl-methionyl-leucyl-phenylalanine (fMLP) and SiO_2 spheres with sizes ranging from 350 to 400 nm were purchased from Sigma-Aldrich. K_2PdCl_4 (99%) was purchased from Sinopharm Chemical Reagent Co. (China). Dopamine hydrochloride (98%) and tris(hydroxymethyl) aminomethane (Tris, 99.8%) were purchased from Aladdin Chemistry Co., Ltd., China.

2.2. Synthesis of Pd@Co_3O_4 Hollow Spheres. For the synthesis of SiO_2@PDA spheres, 1000 mg of the SiO_2 (350−400 nm) was immersed in 100 mL of 3 mg/mL dopamine Tris solution (pH 8.5, 10 mM Tris buffer) and allowed to proceed for 48 h under stirring at room temperature.[35] The resultant product was separated and collected and subsequently put through five wash cycles and dried by freeze-drying. A 900 mg portion of as-synthesized SiO_2@PDA was dispersed in 75 mL of DI water; then, 70 mg of K_2PdCl_4 was added, and the mixture was kept in a vial under vigorous stirring for 30 min in an ice bath.[36] The mixture was stirred at 0 °C for 30 min. After the reaction, the resulting Pd-NP-deposited SiO_2@PDA was separated from the suspension, and subsequently washed with ultrapure water five times and dried by freeze-drying. The content of Pd NPs in SiO_2@PDA@Pd can be adjusted by changing the amount of precursor K_2PdCl_4 that was added in the SiO_2@PDA aqueous dispersion. The resulting SiO_2@PDA@Pd composites were carbonized at 500 °C for 3 h under an inert atmosphere. Finally, SiO_2 cores were etched by HF solution (≈4%) to get C@Pd hollow spheres.[37] Then, C@Pd (20 mg) was dispersed in toluene (1.6 mL). $Co_2(CO)_8$ (12.4 mg) in toluene (6 mL) was added. The reaction mixture was heated at 100 °C overnight. During this process, the dark solution became transparent. The resultant dark yellow solids were retrieved by centrifugation, washed with toluene, and dried under a vacuum for 3 h. Then, the solids were heated at 500 °C for 5 h under air to form black powders,[26] and the Pd@Co_3O_4 hollow spheres were obtained. The Co_3O_4 hollow spheres were prepared under the same procedure but without the addition of K_2PdCl_4 in the SiO_2@PDA dispersion.

2.3. Fabrication of a Hollow Nanospheres Modified Electrode. The as-obtained Pd@Co_3O_4 powdery sample was dispersed in deionized water with ultrasonic agitating for a few minutes to give a 1.0 mg mL^{-1} black suspension. Then, 10 μL of the suspension was dropped on a cleaned glass carbon electrode (GCE) and the solvent was evaporated in air; thus, a uniform film coated electrode (Pd@Co_3O_4/GCE) was obtained. The C@Pd/GCE was fabricated through a similar method. The as-prepared Pd@Co_3O_4/GCE and C@Pd/GCE were washed carefully with deionized water and then dried at room temperature. All the experiments were processed at room temperature. Before the electrochemical measurement, the nanohybird electrodes were activated by cyclic voltammetric (CV) scanning for 20 cycles in the potential range from −0.4 to +1.0 V versus saturated calomel electrode (SCE).

2.4. Cell Culture and Detection of Extracellular Release of H_2O_2. In this work, three types of living human cells, i.e., human cervical carcinoma Hela cell, RSC96 Schwann cells, and human umbilical vein endothelial cells (HUVEC), were obtained from Center for Tissue Engineering and Regenerative Medicine, Union Hospital,

DOI: 10.1021/acsami.5b00600
ACS Appl. Mater. Interfaces 2015, 7, 5583−5590

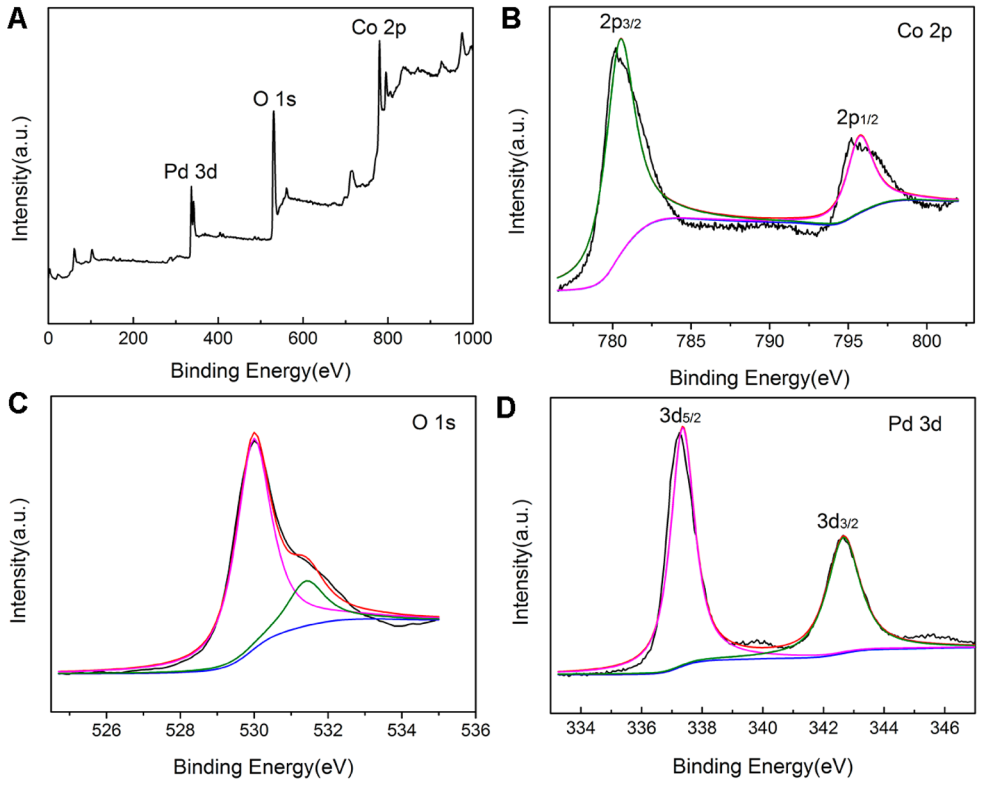

Figure 2. (A) XPS survey spectrum of Pd@Co_3O_4 hollow spheres. Curve fit of (B) Co 2p, (C) O 1s, and (D) Pd 3d spectra of Pd@Co_3O_4 hollow spheres.

HUST (Wuhan, China). The cells were maintained in a culture medium consisting of Dulbecco's modified Eagle medium (DMEM) at 37 °C and subcultured every 3 days. After centrifuging, the cells were planted at a confluency of 80% and used for the electrochemical experiments. To detect the secretion of H_2O_2 by living cells, Pd@Co_3O_4/GCE was used as the working electrode and located near the living cell lines in a culture medium consisting of DMEM at 37 °C. The well containing no living cells was used as the control. For electrochemical experiments, 10 μL of *N*-formyl-methionyl-leucyl-phenylalanine (fMLP, 0.1 mM) was injected into the testing wells and control wells, and the amperometric current responses at the applied potential of 0.6 V were recorded.

2.5. Characterization. CV and chronoamperometric experiments were performed with a CHI660E electrochemical workstation (CH Instrument Company, Shanghai, China). A conventional three-electrode system was adopted. The working electrode was a modified electrode, and the auxiliary and reference electrodes were Pt foil and SCE, respectively. Transmission electron microscopy (TEM) and high-resolution transmission electron microscopy (HRTEM) images were obtained using a TECNAI G2 20 U-Twin instrument (Netherlands) operated at an acceleration voltage of 200 kV. The samples were suspended in ethanol and were prepared by being drop-cast onto a carbon-coated 200-mesh copper grid and subsequently dried at room temperature. X-ray photoelectron spectroscopy (XPS) was performed with an ESCALAB MKII spectrometer (VG Co., U.K.), using Mg Kα radiation (1253.6 eV) at a pressure of 2.0×10^{-10} mbar. The peak positions were internally referenced to the C 1s peak at 284.6 eV. The Pd content in the sample was determined using a microwave plasma-atom emission spectrometer (MP-AES, Agilent 4100, USA). The fluorescence microscope (Olympus IX71, Japan) equipped with a DP73 camera was used to examine sericin scaffolds under the light with the different wavelengths. The images were taken with the software cellSens standard 1.7 (Olympus, Japan).

3. RESULTS AND DISCUSSION

For the synthesis of Pd@Co_3O_4, the SiO_2 spheres with a good monodispersity and a uniform diameter of 350−400 nm (Figure 1A and Figure S1, Supporting Information) were first immersed in 3 mg/mL dopamine (DA) Tris solution for 48 h. During this procedure, DA will self-polymerize to form a transparent polydopamine (PDA) layer that wrapped on SiO_2 spheres (SiO_2@PDA), as shown in the transmission electron microscopy (TEM) of Figure 1B. Previous studies have demonstrated that PDA contained a certain amount of catechol groups, which are able to release electrons when oxidized into the corresponding quinone group and trigger reduction processes of metallic cations.[38,39] Consequently, it can be used as a reducing agent to prepare PDA−NP composites via direct redox reaction with metal salt under the mild condition. In this work, K_2PdCl_4 was added into the SiO_2@PDA suspension under vigorous stirring for 30 min at 0 °C, upon which the spontaneous redox reaction between K_2PdCl_4 and PDA occurs, leading to the formation of ultrafine Pd NPs, which were fairly well-distributed on the surface of the SiO_2@PDA sphere (Figure 1C). The as-obtained Pd NPs decorated SiO_2@PDA (SiO_2@PDA@Pd) spheres were carbonized at 500 °C for 3 h under an inert atmosphere. Then, the SiO_2 cores were etched by HF solution (~4%) to form unique C@Pd hollow spheres, which was confirmed by TEM image (Figure 1D) and scanning electron microscopy (SEM) image (Figure S2, Supporting Information). From the high-resolution TEM (HRTEM) image, it can be observed that numerous ultrafine Pd NPs are dispersed on the surface of hollow spheres, with a mean size of ~2 nm (Figure 1D, inset). The successful synthesis of C@Pd was further confirmed by the energy dispersive X-ray spectroscopy (EDX), which demonstrates the

DOI: 10.1021/acsami.5b00600
ACS Appl. Mater. Interfaces 2015, 7, 5583−5590

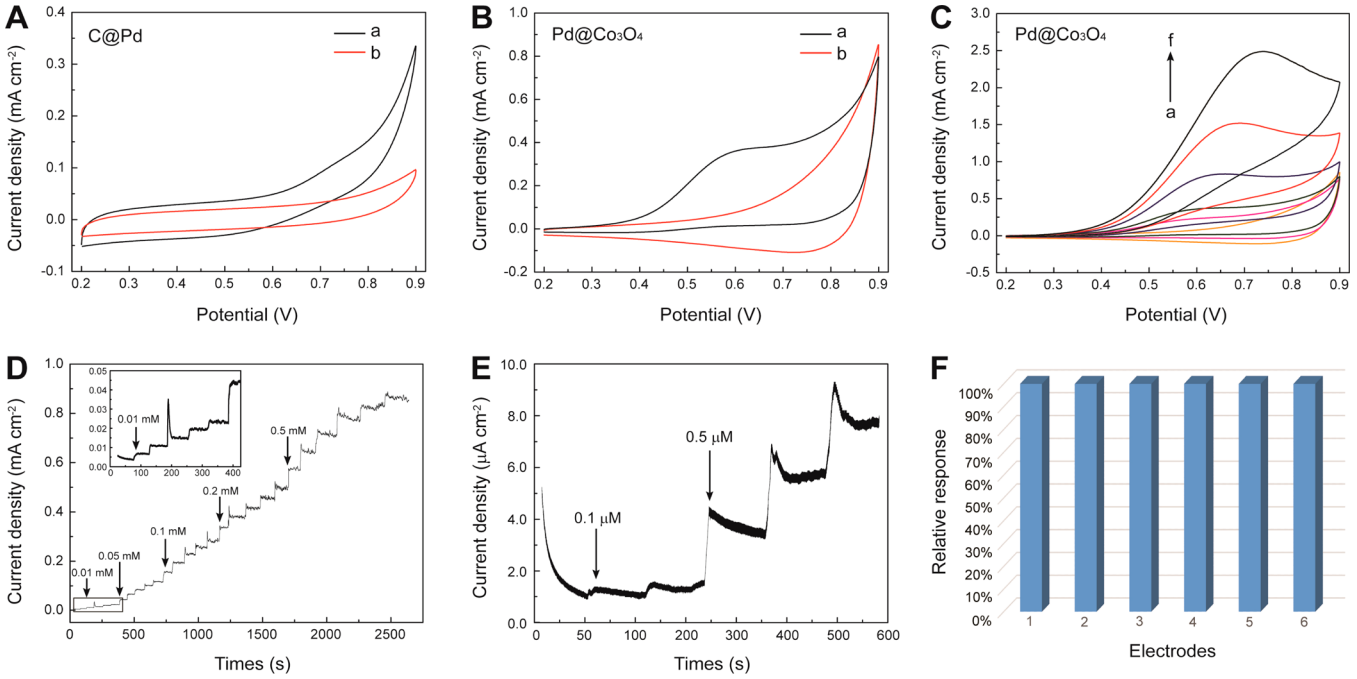

Figure 3. CV curves of (A) C@Pd/GCE and (B) Pd@Co_3O_4/GCE in 0.1 M PBS (pH 7.4) in the presence (A) and absence (B) of H_2O_2 (2 mM). (C) CV curves of Pd@Co_3O_4/GCE in 0.1 M PBS (pH 7.4) in the presence of H_2O_2 with different concentrations (from a to f: 0, 1, 2, 5, 10, 20 mM). Scan rate: 50 mV s^{-1}. (D) Typical amperometric response of Pd@Co_3O_4/GCE to successive addition of 0.01, 0.05, 0.1, 0.2, and 0.5 mM H_2O_2 in stirring PBS buffer (pH 7.4). The inset shows the partial enlarged curves. (E) Amperometric response of Pd@Co_3O_4/GCE to successive addition of 0.1 and 0.5 μM H_2O_2 in stirring PBS buffer (pH 7.4). (F) Amperometric response of six different Pd@Co_3O_4/GCEs to 0.1 mM H_2O_2. Applied potential: 0.6 V.

presence of C and Pd elements in the hollow spheres (Figure S3, Supporting Information). The content of Pd in C@Pd hollow nanospheres has been determined to be 2.08 wt % using MP-AES. The C@Pd hollow spheres were redispersed in toluene. After addition of $Co_2(CO)_8$ in C@Pd suspension, the reaction mixture was heated at 100 °C overnight, and the dark solution became transparent. The resultant dark yellow solids were retrieved by centrifugation, washed with toluene, and dried under a vacuum for 3 h. Then, the solids were heated at 500 °C for 5 h under air to form black powders. In this process, the C@Pd hollow spheres were converted to Pd@Co_3O_4 hollow spheres, which also exhibit a good monodispersity and a uniform diameter of 350−400 nm (Figure S4, Supporting Information). The content of Pd in Pd@Co_3O_4 hollow nanospheres is as low as 1.14 wt % using MP-AES measurement. Moreover, it can be observed that the Pd@Co_3O_4 hollow spheres contain microporous shells (Figure 1E and Figure S5, Supporting Information). Figure 1F shows the HRTEM image of Pd@Co_3O_4 hollow spheres, which indicates that the microporous shells actually consist of many tiny NPs. These NPs have a single crystalline structure extending along the Co(111) direction, with a lattice spacing of 0.467 nm.[40] And the single crystalline Pd(200) NPs with a lattice spacing of 0.222 nm are encapsulated in the Co_3O_4 microporous shells.[41] The XRD pattern further demonstrates that Pd@Co_3O_4 hollow spheres exhibit six diffraction peaks corresponding to the (111), (220), (311), (400), (422), and (440) facets of cubic Co_3O_4 (JCPDS 74-2120). However, owing to the ultrafine size (~2 nm) and low content (1.14 wt %) of Pd NP Pd@Co_3O_4 hollow spheres, their diffraction peaks are undetectable in the XRD patterns recorded in the 2θ range of 10−90° (Figure S6, Supporting Information).

The surface chemical compositions and the valence states of samples are further investigated by the X-ray photoelectron spectroscopy (XPS). As shown in Figure 2A, the XPS spectrum of the Pd@Co_3O_4 sample exhibits three main peaks centered at the Co, O, and Pd core level regions, which are assigned to Co 2p, O 1s, and Pd 3d, respectively. The deconvoluted Co 2p XPS spectrum shown in Figure 2B exhibits two characteristic broad peaks encompassing the Co^{2+}/Co^{3+} $2p_{3/2}$ and Co^{2+}/Co^{3+} $2p_{1/2}$ states at 780.4 and 795.7 eV, respectively. The deconvoluted peaks centered at 530.0 and 531.4 eV can be observed in Figure 2C, which correspond to the oxygenated groups. These results combined suggest the formation of the standard Co_3O_4 phase.[27] The deconvoluted Pd 3d XPS spectrum exhibits two distinct peaks at 337.4 and 342.7 eV, respectively (Figure 2D), which are in good agreement with the reported XPS data of Pd $3d_{5/2}$ and Pd $3d_{3/2}$ in PdO.[42]

To evaluate the electrochemical sensing performance of Pd@Co_3O_4 nanospheres, the powdery Pd@Co_3O_4 sample was dispersed in deionized water and modified on the clean glass carbon electrode (GCE) to fabricate the Pd@Co_3O_4 modified GCE (Pd@Co_3O_4/GCE). For comparison, the C@Pd/GCE was also prepared under the same procedure. Figure 3A shows the cyclic voltammetric (CV) behaviors of C@Pd/GCE in the absence and presence of 2.0 mM H_2O_2 in 0.1 M phosphate buffer solution (PBS) at a scan rate of 50 mV s^{-1}. In blank PBS (pH 7.4), the CV curve of Pd@Co_3O_4/GCE does not display any visible peaks in the potential range from 0.2 to 0.9 V. In the presence of 2 mM H_2O_2, a well-defined anodic peak that is associated with the oxidation of H_2O_2 can be observed at 0.58 V on Pd@Co_3O_4/GCE (Figure 3B). Along with increased concentration of H_2O_2 from 1.0 to 20 mM, the oxidation peak currents also increase dramatically (Figure 3C). In contrast, C@Pd/GCE gives rise to an inconspicuous oxidation peak at

DOI: 10.1021/acsami.5b00600
ACS Appl. Mater. Interfaces 2015, 7, 5583−5590

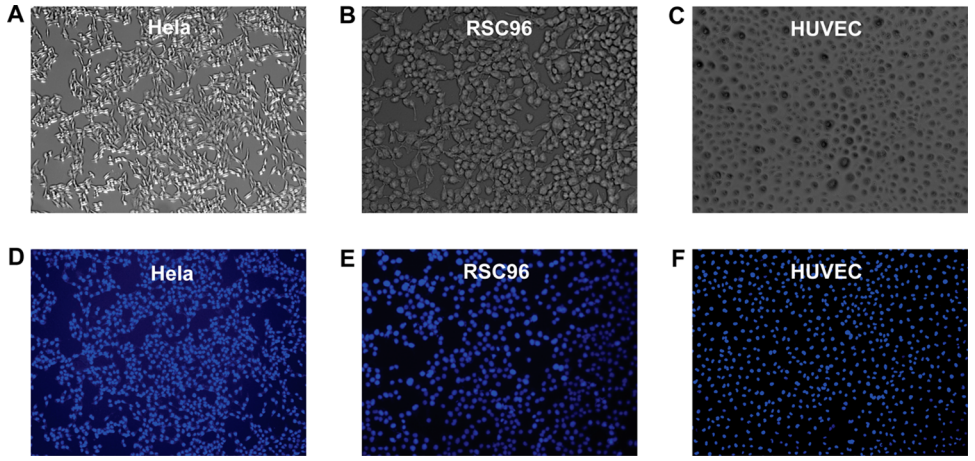

Figure 4. Bright-field image (A–C) and dark-field image (D–F) of Hela cell, RSC96 Schwann cells, and HUVEC cells used in the in vitro tests.

0.75 V in 0.1 M PBS containing 2.0 mM H_2O_2, which is 130 mV more positive than that of Pd@Co_3O_4/GCE. However, under the same condition, there are not any obvious redox peaks of H_2O_2 observed at Co_3O_4/GCE, in comparison with those without H_2O_2. These indicate that the Pd@Co_3O_4/GCE possesses high electrocatalytic activity toward H_2O_2 oxidation by taking advantage of the high electrocatalytic activity of Pd NPs on Co_3O_4 hollow spheres, as well as the synergistic effect between Pd NPs and Co_3O_4 hollow spheres, even when the content of Pd in Pd@Co_3O_4 hollow nanospheres is as low as 1.14 wt %.

Furthermore, the relationship between the electrocatalytic activity of Pd@Co_3O_4 hollow nanospheres toward the oxidation of H_2O_2 and Pd mass content in Pd@Co_3O_4 hollow nanospheres has also been investigated. For the preparation of Pd@Co_3O_4 hollow nanospheres, the Pd mass content in Pd@Co_3O_4 nanocomposites can be originally adjusted by changing the amount of precursor K_2PdCl_4 that is added in SiO_2@PDA aqueous dispersion. The results show that the amperometric current responses of Pd@Co_3O_4/GCE toward 2.0 mM H_2O_2 first increase with precursor K_2PdCl_4 content. However, when the mass ratio of K_2PdCl_4 to SiO_2@PDA reaches 7/90, the amperometric responses tend to decrease (Figure S7, Supporting Information), probably due to the aggregation of Pd NPs on Co_3O_4 hollow nanospheres, which decreases the electrocatalytic activity of Pd@Co_3O_4 hollow nanospheres. Therefore, in this work, the optimal mass ratio of K_2PdCl_4 to SiO_2@PDA is fixed at 7/90 for the further amperometric measure of H_2O_2.

Figure 3D presents the amperometric responses of Pd@Co_3O_4/GCE for successive addition of H_2O_2 under an applied potential at 0.6 V in 0.1 M PBS (pH 7.4). Upon each addition of H_2O_2, Pd@Co_3O_4/GCE rapidly attains the maximum steady-state current within 3 s. The amperometric response is linear to H_2O_2 concentration up to 3.3 mM, with a detection limit of 0.1 μM (S/N = 3), as shown in Figure 3E, and detection sensitivity is as high as 0.24 mA cm^{-2} mM^{-1} (Figure S8, Supporting Information). The sensor performances of linear range, detection limit, and sensitivity in this work are superior to those of the previously reported electrochemical sensors based on noble metal catalysts and/or enzyme electrode for the determination of H_2O_2.[43−50] The reproducibility was explored by measuring 0.1 mM H_2O_2 using six different modified electrodes. The results show that the amperometric responses of six different Pd@Co_3O_4/GCEs provide a relative standard deviation (RSD) value less than 5% (Figure 3F). More importantly, the amperometric responses of Pd@Co_3O_4/GCE can maintain over 90% of its initial value after 50 times repeated testing or storage for more than 4 months, indicating the good reproducibility and stability of the proposed nanohybrid electrode for the detection of H_2O_2.

Considering that the selectivity is an important parameter of biosensors, the potential interferences of several foreign species in real cells, including ascorbic acid (AA), uric acid (UA), dopamine (DA), glutamic acid, glycine, glutathione, Na^+, K^+, Mg^{2+}, Ca^{2+}, H^+, and Cl^-, have been investigated. Our results showed that the changes of amperometric responses of 1.0 mM H_2O_2 were less than 10% upon the addition of 1.0 mM AA, UA, DA, glutamic acid, glycine, and glutathione and 5.0 mM Na^+, K^+, Mg^{2+}, Ca^{2+}, H^+, and Cl^- (Table S1, Supporting Information), which indicates that the existence of these foreign species did not cause significant interference on the amperometric detection of H_2O_2, and the nanohybrid electrode possesses high selectivity toward the electrochemical detection of H_2O_2.

The high electrocatalytic activity and superior sensing performance of Pd@Co_3O_4/GCE toward H_2O_2 can be attributed to two factors: On one hand, for the preparation of the Pd@Co_3O_4 precursor, i.e., SiO_2@PDA@Pd sphere, the K_2PdCl_4 was in situ reduced by catechol groups of PDA on a SiO_2 sphere under the mild condition, leading to the formation of ultrafine and low-load Pd NPs, which are well-distributed on the surface of the SiO_2 sphere. For electrocatalytic application, the active metal NPs with fine particle size and uniform size distribution are anticipated to possess a high catalytic activity. On the other hand, for a Pd@Co_3O_4 hollow sphere, the microporous Co_3O_4 shells provide a large surface area for catalytic reaction as well as promote diffusion and mass transfer of reactants. And the Co_3O_4 shells can also prevent the encapsulated Pd NPs from aggregation or leaching by the shell protection, which endow the good stability of the resultant nanohybird electrode.

Owing to the optimal performances of high sensitivity, wide linear range, and good reproducibility, the proposed Pd@Co_3O_4 based biosensor was used for in vitro tracking of H_2O_2 secretion by living cells. In this work, three types of living human cells, i.e., human cervical carcinoma Hela cells, RSC96 Schwann cells, and human umbilical vein endothelial cells (HUVEC), were chosen for real-time electrochemical determination of H_2O_2 released upon being stimulated. The Hela cell

DOI: 10.1021/acsami.5b00600
ACS Appl. Mater. Interfaces 2015, 7, 5583−5590

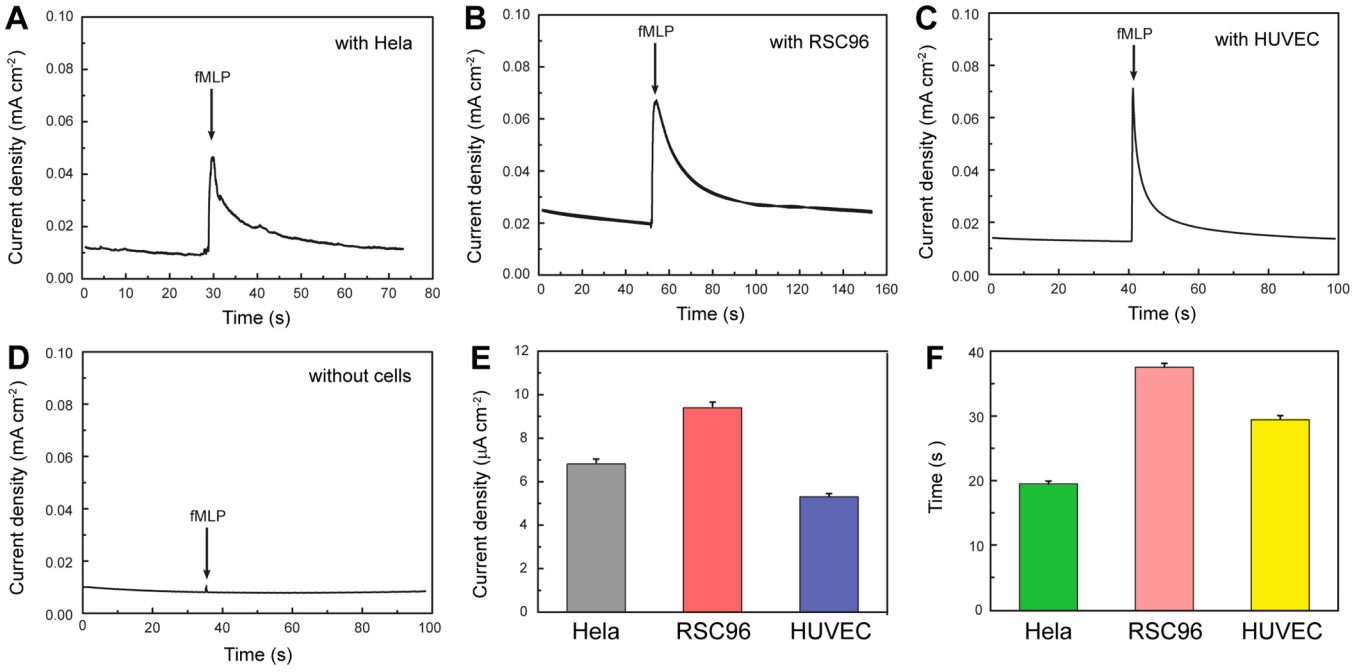

Figure 5. Amperometric responses of Pd@Co_3O_4/GCE in 0.1 M PBS (pH 7.4) with the addition of 10 μL fMLP (0.1 mM) in the presence of (A) Hela cell, (B) RSC96 Schwann cells, and (C) HUVEC cells and (D) in the absence of cells. (E) The increased amperometric responses of three types of living cells upon the addition of 10 μL of fMLP (0.1 mM). (F) The response times to reach the plateau for three types of living cells.

line that derived from human cervical cancer cells is of great significance in cervical cancer diagnosis and treatment.[51] The RSC96 cell line that derived from the glia of the peripheral nervous system is commonly used in nerve biologic research.[52] And the HUVEC line that derived from the umbilical cord is used as a laboratory model system to study the function and pathology of endothelial cells.[53] Considering the different derivation and function of these three types of living human cells, the systematic study of their responses under the stimulation will be of great significance in physiological and pathological investigations. Figure 4 shows the bright-field and dark-field microscope images of Hela cells, RSC96 cells, and HUVEC cells after being incubated with the Pd@Co_3O_4/GCE for over 2 h, which demonstrates that these three cells still maintained their activity, and did not show any changes in cell morphology and viability, indicating the good biocompatibility of Pd@Co_3O_4/GCE.

The live cells of 80% confluency are induced to release H_2O_2 by injecting fMLP, which is one of the synthetic *N*-formyl methionyl peptides that can simulate the secretion of several effector molecules including interleukin 1, lysosomal enzymes, tumor necrosis factor, nitric oxide, and reactive oxygen intermediates (ROI) by living cells.[54] Figure 5A–C depicts the amperometric response changes of Pd@Co_3O_4/GCE located near the living cell lines in a culture medium consisting of Dulbecco's modified Eagle medium (DMEM) at 37 °C. After injection of 10 μL of fMLP (0.1 mM), a significant increased current is observed for all the living cells at an applied potential of 0.6 V, followed by a gradual decrease of current, which finally reaches a plateau. However, the control wells containing no living cells do not generate any signal response to the addition of fMLP (Figure 5D). These results together suggest that the generated increase of amperometric responses is ascribed to the electrochemical reduction of H_2O_2 released by living cells upon being stimulated by fMLP. Moreover, the increased current densities and the times to reach the plateau for these three types of living cells are investigated in detail. As shown in Figure 5E and 5F, upon the addition of an equal amount of fMLP, the increased amperometric current densities for Hela cells, RSC96 cells, and HUVEC cells are 6.9, 9.2, and 5.3 μA cm^{-2}, respectively. And the response times to reach the plateau for these cells also increase in the order of RSC96 cells > HUVEC cells > Hela cells. These observations substantially demonstrate that the proposed biosensor based on Pd@Co_3O_4/GCE establishes a simple, fast, and reliable method for the quantitative determination of H_2O_2 secreted by different living cells.

4. CONCLUSIONS

In summary, we have demonstrated the design and synthesis of a new type of high-performance nanocatalyst, i.e., microporous Pd@Co_3O_4 hollow nanosphere, and explored its practical application as an electrode material in an electrochemical sensor for in situ molecular detection of living cells. Owing to the synergy effect between the permeable microporous Co_3O_4 shell and the active Pd NPs that encapsulated in it, the resultant Pd@Co_3O_4 based biosensor shows significantly improved electrochemical sensing performance toward H_2O_2, even when the content of active Pd NPs in a Pd@Co_3O_4 hollow nanosphere is as low as 1.14 wt %. These enable it to be used for real-time tracking of the secretion of H_2O_2 in living human cells. The modular nature of this approach coupled with recent progress in core–shell hollow nanosphere synthesis and electrocatalysis opens new possibilities to systematically study the dependence of catalytic performance on the structural parameters and chemical compositions of the core–shell hollow nanosphere catalysts. Therefore, it is envisioned that the fabrication of Pd@Co_3O_4 provides a blueprint for designing various nanocatalysts encapsulated in microporous hollow sphere structures, which will be quite promising for a wide range of applications in catalysis, drug/gene delivery, and energy storage systems.

DOI: 10.1021/acsami.5b00600
ACS Appl. Mater. Interfaces 2015, 7, 5583–5590

■ ASSOCIATED CONTENT

Supporting Information

SEM images of C@Pd hollow spheres and Pd@Co_3O_4 hollow spheres, TEM images of SiO_2 spheres and Pd@Co_3O_4 hollow spheres, EDX image of C@Pd hollow spheres, XRD pattern of Pd@Co_3O_4 hollow nanospheres, the relationship curves between the amperometric current responses of Pd@Co_3O_4/GCE toward 2.0 mM H_2O_2 and mass ratio of K_2PdCl_4 to SiO_2@PDA, calibration curves of the amperometric response of Pd@Co_3O_4/GCE to successive addition of H_2O_2 in stirring PBS buffer (pH 7.4), and the table of influence of foreign species on the determination of 1.0 mM H_2O_2. This material is available free of charge via the Internet at http://pubs.acs.org.

■ AUTHOR INFORMATION

Corresponding Authors

*E-mail: xiaofei@hust.edu.cn.

*E-mail: chmsamuel@mail.hust.edu.cn.

Author Contributions

§J.X., Y.Z.: These authors contributed equally.

Notes

The authors declare no competing financial interest.

■ ACKNOWLEDGMENTS

This research was financially supported by the National Natural Science Foundation of China (Grant Nos. 51173055 and 21305048) and National Program on Key Basic Research Project (973 Program, Grant No. 2013CBA01600).

■ REFERENCES

(1) Luo, Y. P.; Liu, H. Q.; Rui, Q. Y. Tian, Detection of Extracellular H_2O_2 Released from Human Liver Cancer Cells Based on TiO_2 Nanoneedles with Enhanced Electron Transfer of Cytochrome c. *Anal. Chem.* **2009**, *81*, 3035−3041.

(2) Luo, Y. P.; Tian, Y.; Rui, Q. Electrochemical Assay of Superoxide Based on Biomimetic Enzyme at Highly Conductive TiO_2 Nanoneedles: From Principle to Applications in Living Cells. *Chem. Commun.* **2009**, *21*, 3014−3016.

(3) Miller, E. W.; Dickinsion, B. C.; Chang, C. J. Aquaporin-3 Mediates Hydrogen Peroxide Uptake to Regulate Downstream Intracellular Signaling. *Proc. Natl. Acad. Sci., India* **2010**, *7*, 15681−15686.

(4) Yuan, L.; Lin, W.; Xie, Y.; Chen, B.; Zhu, S. Single Fluorescent Probe Responds to H_2O_2, NO, and H_2O_2/NO with Three Different Sets of Fluorescence Signals. *J. Am. Chem. Soc.* **2012**, *134*, 1305−1315.

(5) Xu, J.; Li, Q.; Yue, Y.; Guo, Y.; Shao, S. J. A Water-soluble BODIPY Derivative as a Highly Selective "Turn-On" Fluorescent Sensor for H_2O_2 Sensing in Vivo. *Biosens. Bioelectron.* **2014**, *56*, 58−63.

(6) Luo, W.; Abbas, M. E.; Zhu, L.; Deng, K.; Tang, H. Rapid Quantitative Determination of Hydrogen Peroxide by Oxidation Decolorization of Methyl Orange Using a Fenton Reaction System. *Anal. Chim. Acta* **2008**, *629*, 1−5.

(7) Effkemann, S.; Pinkernell, U.; Neumuller, R.; Schwan, F.; Engelhardt, H.; Karst, U. Liquid Chromatographic Simultaneous Determination of Peroxycarboxylic Acids Using Postcolumn Derivatization. *Anal. Chem.* **1998**, *70*, 3857−3862.

(8) Šljukiæ, B.; Banks, C. E.; Compton, R. G. Iron Oxide Particles Are the Active Sites for Hydrogen Peroxide Sensing at Multiwalled Carbon Nanotube Modified Electrodes. *Nano Lett.* **2006**, *6*, 1556−1558.

(9) Li, J. W.; Liu, L. H.; Xiao, F.; Gui, Z.; Yan, R.; Zhao, F. Q.; Hu, L.; Zeng, B. Z. Direct Electron Transfer and Electrocatalysis of Horseradish Peroxidase Immobilized in Gemini Surfactant−Ionic Liquid Composite Film on Glassy Carbon Electrode. *J. Electroanal. Chem.* **2008**, *613*, 51−57.

(10) Li, P.; Ding, Y.; Lu, Z. Y.; Chen, Y.; Zhou, Y. M.; Tang, Y. W.; Cai, C. X.; Lu, T. H. An ultrasensitive Iron(III)-complex Based Hydrogen Peroxide Electrochemical Sensor Based on A Non-electrocatalytic Mechanism. *Anal. Chim. Acta* **2013**, *786*, 34−38.

(11) Lin, L.; Yan, J.; Li, J. H. Small-Molecule Triggered Cascade Enzymatic Catalysis in Hour-Glass Shaped Nanochannel Reactor for Glucose Monitoring. *Anal. Chem.* **2014**, *86*, 10546−10551.

(12) Lippert, A. R.; DeBittner, G. C. V.; Chang, C. J. Boronate Oxidation as a Bioorthogonal Reaction Approach for Studying the Chemistry of Hydrogen Peroxide in Living Systems. *Acc. Chem. Res.* **2011**, *44*, 793−804.

(13) Zhou, L. Z.; Kuai, L.; Li, W. Z.; Geng, B. Y. Ion-Exchange Route to Au-Cu_xOS Yolk-Shell Nanostructures with Porous Shells and Their Ultrasensitive H_2O_2 Detection. *ACS Appl. Mater. Interfaces* **2012**, *4*, 6463−6467.

(14) Mazumder, V.; Sun, S. H. Oleylamine-Mediated Synthesis of Pd Nanoparticles for Catalytic Formic Acid Oxidation. *J. Am. Chem. Soc.* **2009**, *131*, 4588−4589.

(15) Huang, X. Q.; Tang, S. H.; Zhang, H. H.; Zhou, Z. Y.; Zheng, N. F. Controlled Formation of Concave Tetrahedral/Trigonal Bipyramidal Palladium Nanocrystals. *J. Am. Chem. Soc.* **2009**, *131*, 13916−13917.

(16) Lee, H. J.; Habas, S. E.; Somorjai, G. A.; Yang, P. D. Localized Pd Overgrowth on Cubic Pt Nanocrystals for Enhanced Electrocatalytic Oxidation of Formic Acid. *J. Am. Chem. Soc.* **2008**, *130*, 5406−5407.

(17) Han, M.; Liu, S. L.; Bao, J. C.; Dai, Z. H. Pd Nanoparticle Assemblies−As the Substitute of HRP, in Their Biosensing Applications for H_2O_2 and Glucose. *Biosens. Bioelectron.* **2012**, *31*, 151−156.

(18) Joo, S. H.; Park, J. Y.; Tsung, C. K.; Yamada, Y.; Yang, P.; Somorjai, G. A. Thermally Stable Pt/mesoporous Silica Core-shell Nanocatalysts for High-temperature Reactions. *Nat. Mater.* **2009**, *8*, 126−131.

(19) Lopez-Sanchez, J. A.; Dimitratos, N.; Hammond, C.; Brett, G. L.; Kesavan, L.; White, S.; Miedziak, P.; Tiruvalam, R.; Jenkins, R. L.; Carley, A. F.; Knight, D.; Kiely, C. J.; Hutchings, G. J. Facile Removal of Stabilizer-ligands from Supported Gold Nanoparticles. *Nat. Chem.* **2011**, *3*, 551−556.

(20) Yoon, K.; Yang, Y.; Lu, P.; Wan, D. H.; Peng, H. C.; Masias, K. S.; Fanson, P. T.; Campbell, C. T.; Xia, Y. N. A Highly Reactive and Sinter-Resistant Catalytic System Based on Platinum Nanoparticles Embedded in the Inner Surfaces of CeO_2 Hollow Fibers. *Angew. Chem., Int. Ed.* **2012**, *51*, 9543−9546.

(21) Bo, X. J.; Bai, J.; Ju, J.; Guo, L. P. A Sensitive Amperometric Sensor for Hydrazine and Hydrogen Peroxide Based on Palladium Nanoparticles/onion-like Mesoporous Carbon Vesicle. *Anal. Chim. Acta* **2010**, *675*, 29−35.

(22) Zhang, F.; Yuan, C. Z.; Zhu, J. J.; Wang, J.; Zhang, X. G.; Lou, X. W. Flexible Films Derived from Electrospun Carbon Nanofibers Incorporated with Co_3O_4 Hollow Nanoparticles as Self-Supported Electrodes for Electrochemical Capacitors. *Adv. Funct. Mater.* **2013**, *23*, 3909−3915.

(23) Lou, X. W. D.; Yuan, C.; Rhoades, E.; Zhang, Q.; Archer, L. A. Encapsulation and Ostwald Ripening of Au and Au−Cl Complex Nanostructures in Silica Shells. *Adv. Funct. Mater.* **2006**, *16*, 1679−1684.

(24) Zhang, G. Q.; Lou, X. W. D. General Synthesis of Multi-Shelled Mixed Metal Oxide Hollow Spheres with Superior Lithium Storage Properties. *Angew. Chem., Int. Ed.* **2014**, *53*, 9041−9044.

(25) Zhang, G. Q.; Lou, X. W. D. General Synthesis of Multi-Shelled Mixed Metal Oxide Hollow Spheres with Superior Lithium Storage Properties. *Angew. Chem., Int. Ed.* **2014**, *53*, 9041−9044.

(26) Jiao, Q.; Fu, Z. M.; You, C.; Zhao, Y.; Li, H. S. Preparation of Hollow Co_3O_4 Microspheres and Their Ethanol Sensing Properties. *Inorg. Chem.* **2012**, *51*, 11513−11520.

(27) Wang, J. Y.; Yang, N. L.; Tang, H. J.; Dong, Z. H.; Jin, Q.; Yang, M.; Kisailus, D.; Zhao, H. J.; Tang, Z. Y.; Wang, D. Accurate Control of Multishelled Co_3O_4 Hollow Microspheres as High-Performance

DOI: 10.1021/acsami.5b00600
ACS Appl. Mater. Interfaces 2015, 7, 5583−5590

Anode Materials in Lithium-Ion Batteries. *Angew. Chem., Int. Ed.* **2013**, *125*, 6545−6548.
(28) Liu, J.; Qiao, S. Z.; Chen, J. S.; Lou, X. W. D.; Xing, X.; Lu, G. Q. M. Yolk/shell Nanoparticles: New Platforms for Nanoreactors, Drug Delivery and Lithium-ion Batteries. *Chem. Commun.* **2011**, *47*, 12578−12591.
(29) Lou, X. W. D.; Archer, L. A.; Yang, Z. C. Hollow Micro-/Nanostructures: Synthesis and Applications. *Adv. Mater.* **2008**, *20*, 3987−4019.
(30) Liu, W.; Liu, J.; Chen, K. F.; Ji, S. M.; Wan, Y. L.; Zhou, Y. C.; Xue, D. F.; Hodgson, P.; Li, Y. C. Enhancing the Electrochemical Performance of the $LiMn_2O_4$ Hollow Microsphere Cathode with a $LiNi_{0.5}Mn_{1.5}O_4$ Coated Layer. *Chem.—Eur. J.* **2014**, *20*, 824−830.
(31) Liu, J.; Liu, W.; Ji, S. M.; Wan, Y. L.; Gu, M. Z.; Yin, H. Q.; Zhou, Y. C. Iron Fluoride Hollow Porous Microspheres: Facile Solution-Phase Synthesis and Their Application for Li-Ion Battery Cathodes. *Chem.—Eur. J.* **2014**, *20*, 5815−5820.
(32) Liu, J.; Liu, W.; Chen, K. F.; Ji, S. M.; Zhou, Y. C.; Wan, Y. L.; Xue, D. F.; Hodgson, P.; Li, Y. C. Facile Synthesis of Transition-Metal Oxide Nanocrystals Embedded in Hollow Carbon Microspheres for High-Rate Lithium-Ion-Battery Anodes. *Chem.—Eur. J.* **2013**, *19*, 9811−9816.
(33) Liu, J.; Xia, H.; Xue, D. F.; Lu, L. Double-shelled Nanocapsules of V_2O_5-Based Composites as High-performance Anode and Cathode Materials for Li Ion Batteries. *J. Am. Chem. Soc.* **2009**, *131*, 12086−12087.
(34) Zhang, N.; Xu, Y. J. Aggregation- and Leaching-Resistant, Reusable, and Multifunctional Pd@CeO_2 as a Robust Nanocatalyst Achieved by a Hollow Core−Shell Strategy. *Chem. Mater.* **2013**, *25*, 1979−1988.
(35) Lee, H.; Dellatore, S. M.; Miller, W. M.; Messersmith, P. B. Mussel-Inspired Surface Chemistry for Multifunctional Coatings. *Science* **2007**, *318*, 426−430.
(36) Guo, L. Q.; Liu, Q.; Li, G. Q.; Shi, J. B.; Liu, J. Y.; Wang, T.; Jiang, G. B. A Mussel-Inspired Polydopamine Coating as A Versatile Platform for the In Situ Synthesis of Graphene-based Nanocomposites. *Nanoscale* **2012**, *4*, 5864−5867.
(37) Zhang, Z. Y.; Xiao, F.; Xi, J. B.; Sun, T.; Xiao, S.; Wang, H. R.; Wang, S.; Liu, Y. Q. Encapsulating Pd Nanoparticles in Double-Shelled Graphene@Carbon Hollow Spheres for Excellent Chemical Catalytic Property. *Sci. Rep.* **2014**, *4*, 4053.
(38) Liu, Y.; Ai, K.; Lu, L. Polydopamine and Its Derivative Materials: Synthesis and Promising Applications in Energy, Environmental, and Biomedical Fields. *Chem. Rev.* **2014**, *114*, 5057−5115.
(39) Ball, V.; Nguyen, I.; Haupt, M.; Oehr, C.; Arnoult, C.; Toniazzo, V.; Ruch, D. The Reduction of Ag^+ in Metallic Silver on Pseudomelanin Films Allows For Antibacterial Activity But Does Not Imply Unpaired Electrons. *J. Colloid Interface Sci.* **2011**, *364*, 359−365.
(40) Xie, X. W.; Li, Y. Z.; Liu, Q.; Haruta, M.; Shen, W. J. Low-temperature Oxidation of CO Catalysed by Co_3O_4 Nanorods. *Nature* **2009**, *458*, 746−749.
(41) Ye, J. Y.; Liu, C. J. $Cu_3(BTC)_2$: CO Oxidation Over MOF Based Catalysts. *Chem. Commun.* **2011**, *47*, 2167−2169.
(42) Gao, X. Q.; Li, F. M.; Li, Y. M.; Li, S. N.; Chen, Y.; Lee, J. M. A Surfactant-free Strategy for Synthesizing Reduced Graphene Oxide Supported Palladium Nanoparticles with Enhanced Electrocatalytic Performance towards Formic Acid Oxidation. *J. Power Sources* **2015**, *280*, 491−498.
(43) Xu, F. G.; Sun, Y. J.; Zhang, Y.; Shi, Y.; Wen, Z. W.; Li, Z. Graphene−Pt Nanocomposite for Nonenzymatic Detection of Hydrogen Peroxide with Enhanced Sensitivity. *Electrochem. Commun.* **2011**, *13*, 1131−1134.
(44) Guascito, M. R.; Chirizzi, D.; Malitesta, C.; Mazzotta, E.; Siciliano, M.; Siciliano, T.; Tepore, A.; Turco, A. Low-potential Sensitive H_2O_2 Detection Based on Composite Micro tubular Te Adsorbed on Platinum Electrode. *Biosens. Bioelectron.* **2011**, *26*, 3562−3569.
(45) Xiao, F.; Song, J. B.; Gao, H. C.; Zan, X. L.; Xu, R.; Duan, H. W. Coating Graphene Paper with 2D-assembly of Electrocatalytic Nanoparticles: A Modular Approach Toward High-performance Flexible Electrodes. *ACS Nano* **2012**, *6*, 100−110.
(46) Chen, K. J.; Pillai, K. C.; Rick, J.; Pan, C. J.; Wang, S. H.; Liu, C. C.; Hwang, B. J. Bimetallic PtM (M = Pd, Ir) Nanoparticle Decorated Multi-walled Carbon Nanotube Enzyme-free, Mediator-less Amperometric Sensor for H_2O_2. *Biosens. Bioelectron.* **2012**, *33*, 120−127.
(47) Han, Y.; Zheng, J.; Dong, S. A Novel Nonenzymatic Hydrogen Peroxide Sensor Based on Ag−MnO_2−MWCNTs Nanocomposites. *Electrochim. Acta* **2013**, *90*, 35−43.
(48) Ji, S.; Guo, Q.; Yue, Q.; Wang, L.; Wang, H.; Zhao, J.; Dong, R.; Liu, J.; Jia, J. Controlled Synthesis of Pt Nanoparticles Array Through Electroreduction of Cisplatin Bound at Nucleobases Terminated Surface and Application into H_2O_2. Sensing. *Biosens. Bioelectron.* **2011**, *26*, 2067−2073.
(49) Miao, Y. E.; He, S.; Zhong, Y.; Yang, Z.; Tjiu, W. W.; Liu, T. A Novel Hydrogen Peroxide Sensor Based on Ag/SnO_2 Composite Nanotubes by Electrospinning. *Electrochim. Acta* **2013**, *99*, 117−123.
(50) Suárez, G.; Santschi, C.; Martin, O. J. F.; Slaveykova, V. Biosensor Based on Chemically-designed Anchorable Cytochrome *c* for the Detection of H_2O_2 Released by Aquaticcells. *Biosens. Bioelectron.* **2013**, *42*, 385−390.
(51) Rahbari, R.; Sheahan, T.; Modes, V.; Collier, P.; Macfarlane, C.; Badge, R. M. A novel L1 Retrotransposon Marker for HeLa Cell Line Identification. *Biotechniques* **2009**, *46*, 277−284.
(52) Ji, Y.; Shen, M.; Wang, X.; Zhang, S.; Yu, S.; Chen, G.; Gu, X.; Ding, F. Comparative Proteomic Analysis of Primary Schwann Cells And a Spontaneously Immortalized Schwann Cell Line RSC 96: A Comprehensive Overview With a Focus on Cell Adhesion and Migration Related Proteins. *J. Proteome Res.* **2012**, *11*, 3186−3198.
(53) Liu, L. S.; Wei, D. H.; Tang, C. K.; Wang, G. X.; Zhang, S. C.; Yin, W. D.; Yang, Y. Z.; Legrand, A. P.; Guidoin, R. A HUVEC Line with a Stable Expression of the VEGF121 Gene to Achieve Complete Endothelialization of Blood Conduits. *Artif. Cells, Blood Substitutes, Immobilization Biotechnol.* **2007**, *35*, 319−331.
(54) Ijzermans, J. N.; Marquet, R. L. Interferon-gamma: A Review. *Immunobiology* **1989**, *179*, 456−473.

DOI: 10.1021/acsami.5b00600
ACS Appl. Mater. Interfaces 2015, 7, 5583−5590